European Journal of Medicinal Chemistry 52 (2012) 111–122

Contents lists available at SciVerse ScienceDirect

European Journal of Medicinal Chemistry

journal homepage: http://www.elsevier.com/locate/ejmech

Original article

A novel series of L-2-benzyloxycarbonylamino-8-(2-pyridyl)-disulfidyloctanoic acid derivatives as histone deacetylase inhibitors: Design, synthesis and molecular modeling study

Dawei Huang, Xiaohui Li*, Yingdong Wei, Zhilong Xiu

School of Life Science and Biotechnology, Dalian University of Technology, No.2 Linggong Road, Dalian 116024, China

ARTICLE INFO

Article history:
Received 26 October 2011
Received in revised form
5 March 2012
Accepted 6 March 2012
Available online 15 March 2012

Keywords:
Histone deacetylase
Histone deacetylase inhibitor
Docking
Molecular dynamics

ABSTRACT

Histone deacetylases inhibitors (HDACIs) have become an attractive class of anticancer agents. In order to find some novel potent HDACIs, we designed and synthesized a series of L-2-benzyloxycarbonylamino-8-(2-pyridyl)-disulfidyloctanoic acid derivatives. All compounds exhibited potent HDAC-inhibitory activity, and two of them had similar potency to TSA. The introduction of 2-amino-4-phenylthiazole or 9-methyleneoxy-fluorenyl group at the surface recognize domain of these HDACIs could greatly increase their HDAC-inhibitory activity. Molecular modeling studies indicated that coordination of the zinc ion by these inhibitors, and formation of hydrogen bond and hydrophobic interaction between inhibitors and HDACs were essential for the HDAC-inhibitory activities of these inhibitors. Asp181, Asp269, Leu276 and Tyr308 in the active site of HDAC2 gave favorable contributions for binding with all compounds.

1. Introduction

The reversible acetylation of the ε-amino groups of lysine residues at the N-terminal domain of histone catalyzed by histone acetyl transferases (HATs) and histone deacetylases (HDACs) is one of the most important chromatin epigenetic modifications [1]. Deacetylation of histone would lead to chromatin condensation, and transcriptional repression is associated with high levels of histone deacetylation. HDACs therefore play a pivotal role in the regulation of gene expression, cell growth and proliferation [2]. Overexpression of HDACs has been linked to the development of cancers in human [3]. Thus, HDAC has become an important target enzyme for anticancer therapies. There are eighteen HDACs in human and these enzymes are subdivided into four classes based on their homologies to yeast HDACs, subcellular localizations and enzymatic activities. Class I includes HDAC1, 2, 3 and HDAC8; Class II has six members, HDAC4-7, HDAC9 and HDAC10; Class III HDACs, also known as Sirtuins, include Sirt1-7, which are NAD^+-dependent enzymes; Class IV which comprises HDAC11, exhibits properties of both class I and class II HDACs [4]. Class I, II and IV are Zn^{2+}-dependent enzymes, and these HDACs are the targets often used for designing anticancer drugs. The structural information of Class I HDACs was obtained from the crystal structures of HDAC-like protein (HDLP) [5], HDAC8 [6] and HDAC2 [7]. Among class I HDACs, HDAC1 and HDAC2 are highly conserved, with about 82% sequence identity between the two proteins. The amino acid residues in the active pockets of both enzymes are identical.

Evidence has shown that treatment of tumor cells with HDAC inhibitors (HDACIs) can arrest cell growth and lead to differentiation and apoptosis [8–10]. Thus research focusing on turning HDACIs into a promising class of anticancer agents is growing [11]. SAHA [12] and FK228 [13] (Fig. 1) have been approved by the US FDA for the treatment of cutaneous T-cell lymphoma (CTCL). A number of other HDACIs, such as valproic acid [14] and MS-275 [15,16] (Fig. 1), are in different phases of clinical trails for the treatment of different cancers.

The classic pharmacophore of HDACIs consists of three distinct domains: metal binding, linker and surface recognition domains [17]. The metal binding domain coordinates the zinc ion in the bottom of the active pocket of HDACs, and it appears to be a precondition for the possession of HDAC-inhibitory activity. The metal binding domain usually comprises a group with metal chelating ability, such as the hydroxamic group [12,18] and thiol group [13,19]. The linker occupies the hydrophobic channel, so hydrophobicity is important for the linker domain. The surface recognition domain is essential for recognizing and binding to the rim of active pocket of enzymes.

In this study, a series of L-2-benzyloxycarbonylamino-8-(2-pyridyl)-disulfidyloctanoic acid derivatives (Fig. 2) were synthesized as HDACIs. These compounds were designed based on the structural features of HDACs. The metal binding domain was

* Corresponding author. Tel.: +86 411 84706326; fax: +86 411 84706369.
E-mail address: lxhxh@dlut.edu.cn (X. Li).

0223-5234/$ – see front matter © 2012 Elsevier Masson SAS. All rights reserved.
doi:10.1016/j.ejmech.2012.03.009

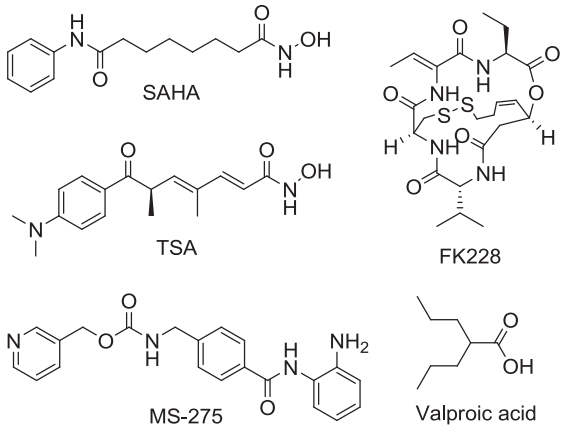

Fig. 1. Structures of some HDACIs.

designed as a thiol group that is protected as a disulfide hybrid [20], but could be reduced to a thiol group by intracellular L-glutathione. The linker domain of these compounds was designed as six methylenes. In the surface recognition domain, some different groups, especial large aromatic groups were introduced at the carboxyl group of L-2-benzyloxycarbonylamino-8-(2-pyridyl)-disulfidyloctanoic acid. Dockings were performed for the binding of the compounds to HDAC2 before they were synthesized to make sure that all compounds could bind to the active pocket of HDACs. After the HDAC-inhibitory and anti-proliferative activities against tumor cells were assessed, molecular dynamics (MD) simulations were conducted to further investigate the interactions between this series of inhibitors and HDACs. Binding free energy was computed by molecular mechanics Poisson–Boltzmann surface area (MM-PBSA) method. Contributions of amino acid residues in the active site of HDAC2 to binding free energy were calculated by molecular mechanics generalized Born surface area (MM-GBSA) method. This study applied molecular modeling to the designing of HDACIs to reveal the structure-activity relationship (SAR) of L-2-benzyloxycarbonylamino-8-(2-pyridyl)-disulfidyloctanoic acid based HDACIs.

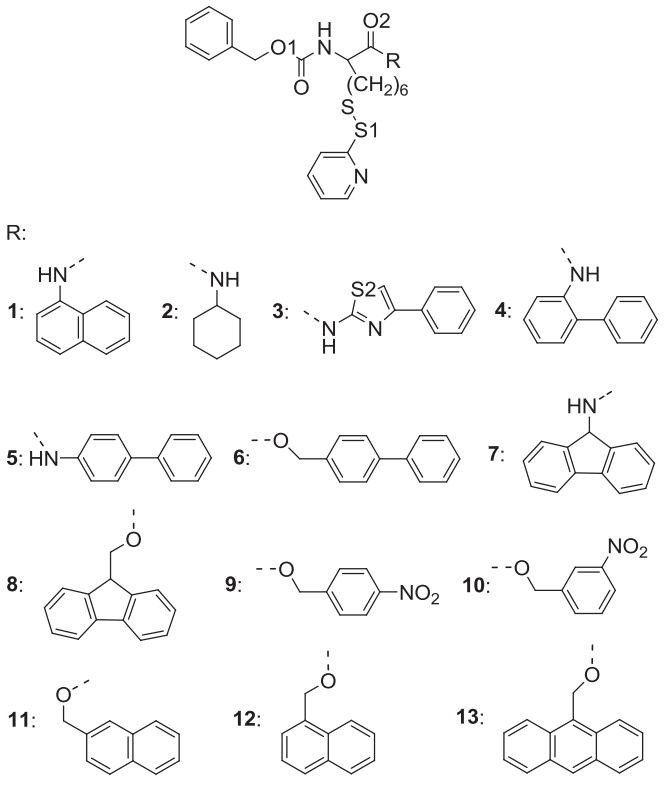

Fig. 2. Structures of designed compounds.

2. Results and discussion

2.1. Docking studies

In order to estimate the rationality of designed compounds and confirm that all of them could bind to the active pocket of HDACs and thus have HDAC-inhibitory activities, all compounds with thiol groups as metal biding domains were docked at the active site of HDAC2 before they were synthesized. As shown in Fig. 3, all compounds were successfully docked into the active pocket. The linker occupied the channel, the surface recognition domain interacted with the rim of the active pocket and the thiol group was at the bottom of the channel. Hydrogen bond and hydrophobic interaction in the binding between the compounds and HDACs enzyme were also examined since these two forces are important in the binding between inhibitor and enzyme. As shown in Fig. 4, when compound **1** is bound to HDAC2, the atoms of the surface recognition domain could hydrogen bond to the amino acid residues in the active site of the enzyme, and the thiol group could interact with the zinc ion that lies in the bottom of the active pocket. Other parts of the compounds made contact with some of the surrounding amino acid residues, such as Phe, Leu, Gly and His via hydrophobic interactions. The results of docking confirmed that these compounds could bind to HDACs. It indicated that the structural differences in the surface recognition domain among these compounds could affect their binding to HDACs. The 1-naphthylamine, cyclohexylamino and 2-amino-4-phenylthiazole groups were introduced to compounds **1**, **2** and **3**, respectively, in order to compare the effect of polycyclic aromatic hydrocarbon, cycloalkane and heterocyclic compound on the interactions between inhibitors and HDACs. The N-terminal benzyloxycarbonyl groups tended to contact the benzene rings of Phe210 or Tyr209 via $\pi-\pi$ interactions, whereas the C-terminal groups bound to the hydrophobic groove formed by His33, Pro34, Phe155 and Leu276, so these rings in the C-terminus had little influence on their bindings to HDAC2. For compounds **4** and **5**, the different substitution sites of biphenyl group had some effect on their interactions with HDAC2. The 2-aminobiphenyl group could contact both Tyr209 and Phe210, but the 4-aminobiphenyl group only interacted with Tyr209. Both benzyloxycarbonyl groups of these two compounds bound to the hydrophobic groove. The C-terminus of compound **6** was an ester, and there was a methylene between the ester bond and benzene ring, so the biphenyl group contacted the hydrophobic groove, and the N-terminal benzyloxycarbonyl group of compound **6** interacted with Tyr209. The N-terminal benzyloxycarbonyl group in compounds **7** and **8** both interacted with Phe210. The C-terminus of compound **7** was 9-aminofluorene, and it bound to the hydrophobic groove. The C-terminus of compound **8** was an ester and there was one more methylene group than compound **7**, and it tended to bind to the groove formed by Tyr209 and Leu276. The 4-nitrobenzyl group of compound **9** contacted Phe210, and the 3-nitrobenzyl group of compound **10** interacted with Leu276 and Arg275. In compound **10**, the nitro group was at the *m*-site, so it could interact with the guanidino group of Arg275 in a good direction. The *o*- or *m*- substitution of naphthalene evidently affected the binding of compounds **11** and **12** to HDAC2. It showed that the 2-naphthylmethyl group of compound **11** bound to the groove formed by Tyr209 and Leu276, but the 1-naphthylmethyl group of compound **12** interacted with Phe210.

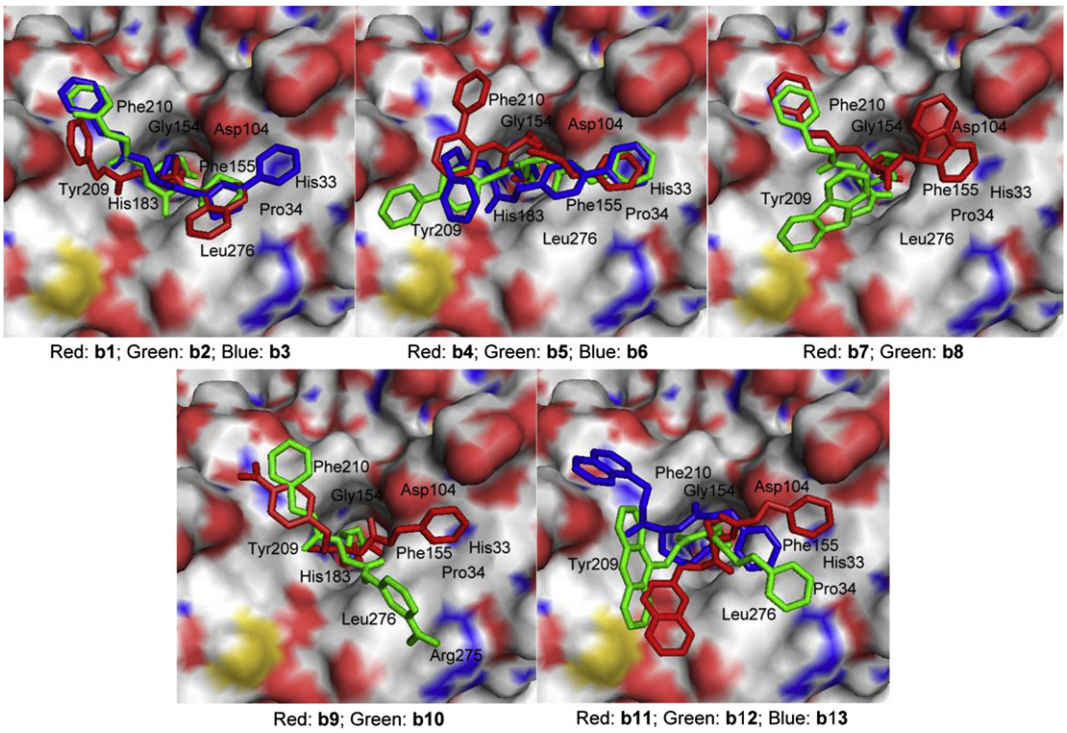

Fig. 3. Top views of the surfaces of the active site region of HDAC2 with compounds from docking.

When the 1-naphthylmethyl group was replaced with a 9-anthracenylmethyl group in compound **13**, it seemed that the 9-anthracenylmethyl group tended to contact Tyr209. The results indicated that there were several sites at the rim of active pocket that could accommodate the surface recognition domains of this series of inhibitors. The structural differences in the C-terminus of these compounds could affect their binding with HDAC2.

2.2. Chemistry

Non-natural amino acid L-2-amino-8-bromooctanoic acid (L-Ab8) was synthesized and its overall yield was 18.2%.

The target compounds were synthesized by the procedure outlined in Scheme 1. All synthesized compounds were confirmed by HRMS, ^{1}H NMR and ^{13}C NMR.

2.3. Biology

The in vitro HDAC-inhibitory activity of all compounds was determined with HDAC Fluorescent Assay/Drug Discovery Kits (AK-511 and AK500, Biomol), and the anti-proliferation activity of all compounds against MCF-7 (human breast cancer cell line) cells was determined by MTT assay. TSA was used as a positive control. All compounds inhibited the activities of HDAC1, HDAC2 and exerted

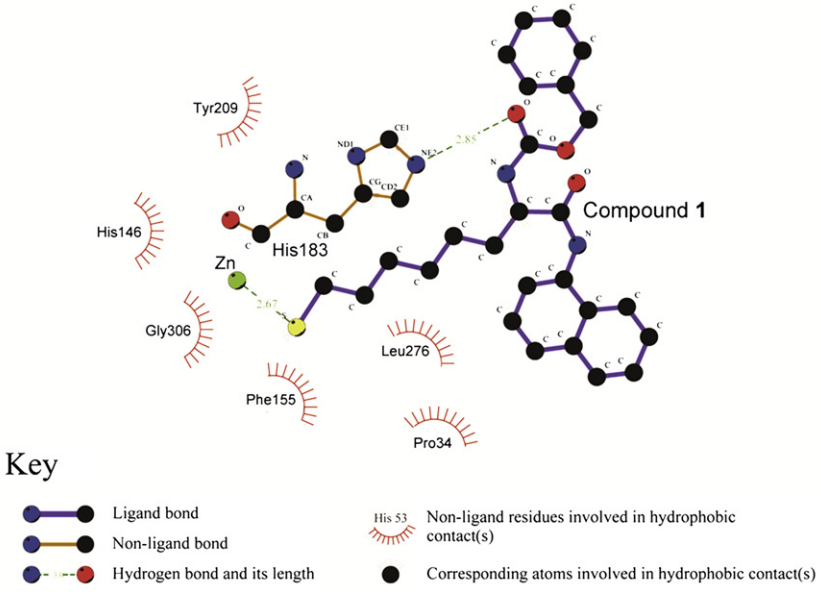

Fig. 4. Hydrogen bonds and hydrophobic contacts between HDAC2 and compound **1**.

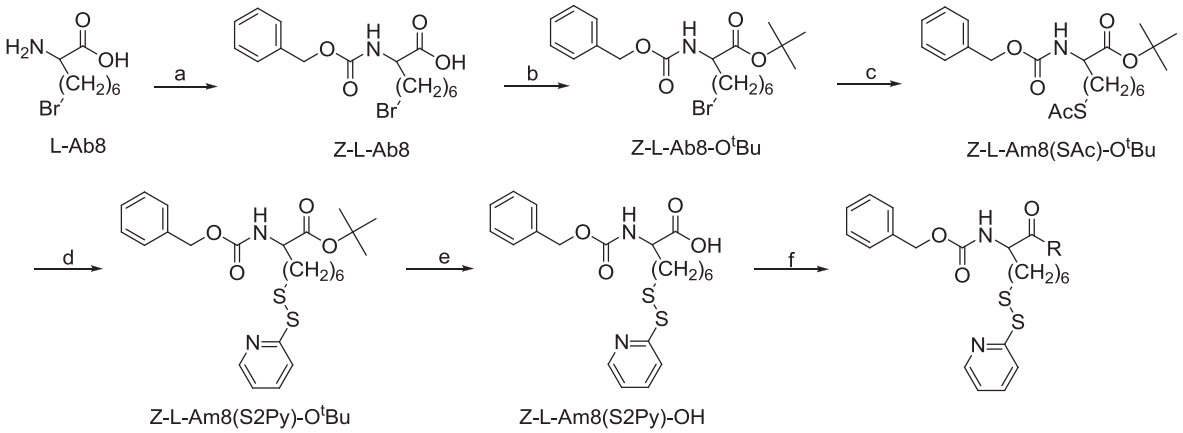

Reagents and conditions: (a) Z-OSu, rt; (b) ^{t}Bu-OH, DMAP, $(Boc)_2O$; (c) AcSK, rt; (d) 2-PDS, CH_3NH_2/MeOH, rt; (e) TFA, 0℃; (f) 1-naphthylamine, HOBt, HBTU, rt (compound **1**); cyclohexylamine, HOBt, HBTU, rt (compound **2**); 2-amino-4-phenylthiazole hydrobromide monohydrate, HOBt, HBTU, rt (compound **3**); 2-aminobiphenyl, HOBt, HBTU, rt (compound **4**); 4-aminobiphenyl, HOBt, HBTU, rt (compound **5**); 4-biphenylmethanol, DMAP, DCC, rt (compound **6**); 9-aminofluorene hydrochloride, HOBt, HBTU, rt (compound **7**); 9-fluorenemethanol, DMAP, DCC, rt (compound **8**); 4-nitrobenzyl bromide, rt (compound **9**); 3-nitrobenzyl bromide, rt (compound **10**); 2-(bromomethyl)naphthalene, rt (compound **11**); 1-naphthalenemethanol, DMAP, DCC, rt (compound **12**); 9-anthracenemethanol, DMAP, DCC, rt (compound **13**)

Scheme 1. Synthetic route of designed compounds.

anti-proliferation activity against MFC-7 cells at low concentrations (Table 1). Compounds **3** and **8** were the most potent compounds, being comparable to TSA. The rest of the compounds exhibited similar HDAC-inhibitory activity, which was about 10 folds less compared to compounds **3** and **8.** They also showed similar anti-proliferative activity against cancer cells. This suggested that introduction of different groups at the C-terminus of L-2-benzyloxycarbonylamino-8-(2-pyridyl)-disulfidyloctanoic acid, which resulted in a change of surface recognition domain could have a substantial effect on HDAC binding. The introduction of 2-amino-4-phenylthiazole (compound **3**) or 9-methyleneoxy-fluorenyl (compound **8**) group at the surface recognition domain could largely increase their HDAC-inhibitory activity. The change between other compounds seemed to have little effect on their HDAC-inhibitory activities.

2.4. MD simulations

To study the interaction between HDAC and each of the synthesized compounds in aqueous solution, MD simulations were conducted for the enzyme–inhibitor complexes using HDAC2 as a representative enzyme. The energetic and structural properties of the complexes were analyzed to explore their dynamic stability. The structures remained stable during the last 500 ps of the simulations for all systems, so all the complexes had converged and reached equilibrium. Atom coordinates in the last 500 ps were chosen to analyze the structure in detail.

Table 1
HDAC-inhibitory and anti-proliferative activities against tumor cells data of synthesized compounds.

Compd.	IC_{50} (μM)		
	HDAC1	HDACs	Cell line (MCF-7)
TSA	0.0023	0.0011	1.7
1	0.0652	0.0382	15.3
2	0.0669	0.0441	19.6
3	0.0051	0.0039	3.2
4	0.0712	0.0452	20.8
5	0.0709	0.0466	18.1
6	0.0641	0.0407	15.6
7	0.0682	0.0481	17.2
8	0.0076	0.0052	3.5
9	0.0644	0.0455	16.9
10	0.0667	0.0485	15.2
11	0.0652	0.0403	14.8
12	0.0647	0.0396	15.3
13	0.0592	0.0436	14.0

Root-mean-squared-fluctuation (RMSF) of C_α, C, N atoms for all complexes were analyzed (Fig. 5). It indicated that all complexes had similar RMSF. Though some amino acid residues in some complexes fluctuated much more than that in other complexes, the conformational changes of the amino acid residues in the active site, especially the residues at the bottom of the channel of HDAC2 (His145, His146, Asp181, His183 and Asp269) were all very small (Fig. 6). It suggested that in HDAC2, some amino acids could shift far away from their normal positions when the enzyme is bound to an inhibitor, but for the amino acids that are in the active site, binding with an inhibitor could make them more rigid.

HDAC2 is a zinc-dependent enzyme, and so the ability of a compound to chelate the zinc ion is a precondition for the inhibition of against the enzyme. The zinc ion coordination states in MD simulations showed that the zinc ion in each complex coordinated five or six atoms, resulting in a pentahedral or hexahedral geometry (Table 2). The carboxylate oxygens of Asp181 and Asp269, and both nitrogen and oxygen atoms of His183 could coordinate the zinc ion. One coordination site was occupied by the sulfur atom of the inhibitor, so coordination of the zinc ion by a sulfur atom was essential for this series of compounds to exert their HDAC-inhibitory activity.

Hydrogen bond formed between a ligand and a protein is very important for stabilizing the ligand–protein complex. In the current MD simulations, the hydrogen bonds between each of the compounds and HDAC2 were examined (Table 3). The result showed that the sulfur atom of each compound could form strong hydrogen bond with Tyr308 of HDAC2, and this gave rise to the potency of these compounds with respect to HDAC inhibition. For compounds **3** and **8**, there was another strong hydrogen bond between the compounds and HDAC2. In compound **3**, the sulfur

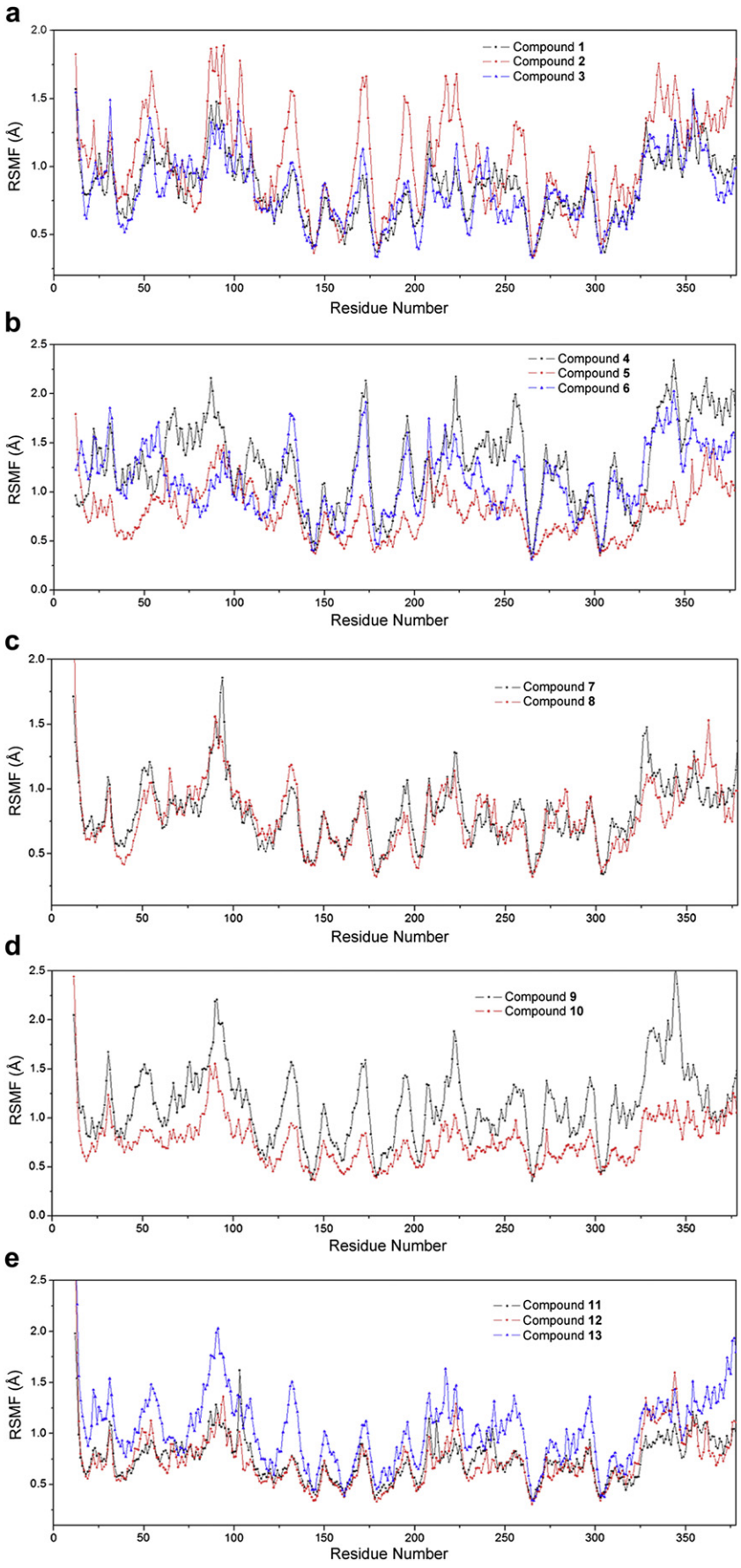

Fig. 5. RMSF for all amino acid residues of HDAC2 during the last 500 ps in MD simulations.

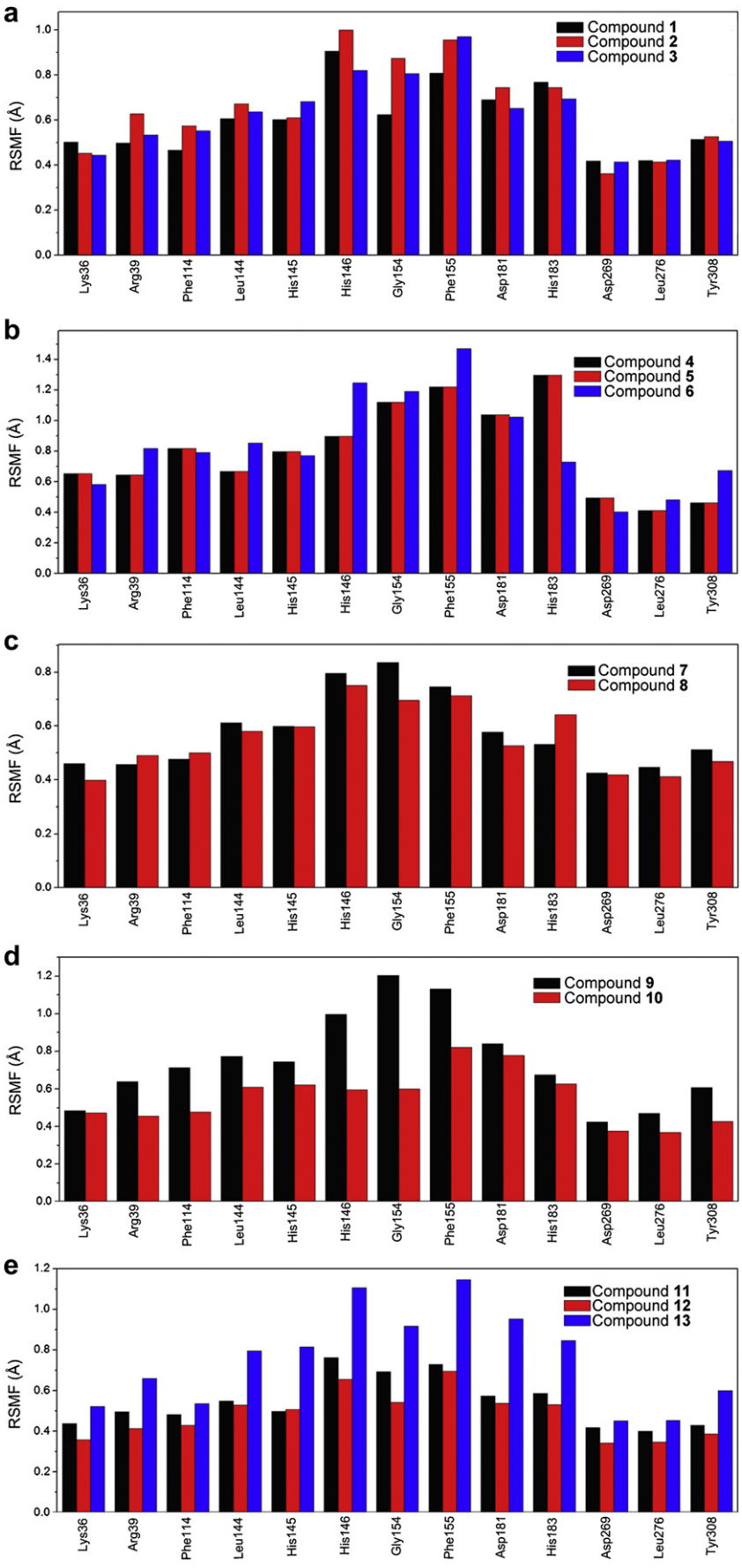

Fig. 6. RMSF for residues in the active site of HDAC2 during the last 500 ps in MD simulations.

Table 2
Average distances between zinc ion and surrounding atoms in HDAC2-compound complexes.

Compd.	Distance (Å)						
	Asp181:OD1	Asp181:OD2	His183:ND1	His183:O	Asp269:OD1	Asp269:OD2	Compd.:S
1	2.60	2.68	2.89	6.15	2.64	2.90	2.79
2	2.72	2.59	2.81	2.90	2.64	4.18	2.79
3	2.63	2.68	5.68	4.75	2.69	2.79	2.84
4	2.61	2.74	2.88	7.25	2.66	2.81	2.82
5	2.71	2.61	2.83	2.89	2.63	4.14	2.79
6	2.70	2.61	2.80	2.91	4.21	2.64	2.77
7	2.62	2.65	2.92	5.18	2.68	2.94	2.81
8	2.70	2.61	2.81	2.82	4.05	2.65	2.80
9	2.68	2.57	2.88	4.90	2.61	3.49	2.79
10	2.66	2.58	2.87	4.87	3.12	2.62	2.77
11	2.63	2.72	2.85	2.84	3.73	2.62	2.82
12	2.66	2.71	2.86	3.54	3.41	2.71	2.78
13	2.59	2.71	2.86	6.65	2.88	2.65	2.79

atom of the metal binding domain also hydrogen bonded with His183. The introduction of a thiazole group at the surface recognition domain may have a large effect on the interaction between the surface recognition domain and the amino acid residues in the rim of the active pocket, and this could further affect the interaction between the metal binding domain and surrounding amino acid residues of HDAC2. In compound **8**, the longer linker of the surface recognition domain could help the carbonyl oxygen to form hydrogen bond with Phe210 of HDAC2. The additional strong hydrogen bonds formed by compound **3** and **8** gave these two compounds higher affinity for HDACs compared to the other compounds.

2.5. Free energy calculation

Free energy associated with the binding of inhibitor to HDAC2 was analyzed by the MM-PBSA method integrated in AMBER9. As shown in Table 4, intermolecular van der Waals (ΔE_{int}^{vdw}) and electrostatics (ΔE_{int}^{ele}) interactions provided major contributions to the binding. non-polar salvation terms (ΔG_{sol}^{nonpol}) also contributed favorably, whereas polar solvation terms (ΔG_{sol}^{ele}) opposed binding. The electrostatic interactions between water molecules and inhibitors were stronger than that between HDAC2 and inhibitors, and therefore the total electrostatic interactions (ΔG_{ele}) were unfavorable for binding. Hydrophobic interaction (ΔG_{sol}^{nonpol}) contributed favorably, and it was more than half of the total binding energy (ΔG_b) for some compounds. This was expected since the linker and surface recognition domains of the inhibitors are hydrophobic, and the active pocket of HDAC2 has some hydrophobic amino acid residues, such as Phe, Tyr and Leu, which can generate strong hydrophobic interaction with these inhibitors. The binding energies of compounds **3** and **8** were much lower compared to the binding energies of the rest of the compounds, and this was in accordance with their higher HDAC-inhibitory activity.

Contributions of the amino acid residues in the active site of HDAC2 to the binding free energy were calculated using MM-GBSA method (Table 5). The results revealed that Asp181, Asp269 Leu276 and Tyr308 were all favorable for binding with all compounds, so these amino acid residues were essential for stabilizing the HDAC2-inhibitor complexes.

Table 3
Hydrogen bonds between the compounds and HDAC2 active site obtained from MD simulations.

Compd.	Donor	AcceptorH	Acceptor	MD simulation	
				Occupied (%)	Distance (Å)
1	Compd. **1**:S	Tyr308:HH	Tyr308:OH	100.00	2.96
2	Compd. **2**:S	Tyr308:HH	Tyr308:OH	100.00	2.89
3	Compd. **3**:S	Tyr308:HH	Tyr308:OH	100.00	2.94
	Compd. **3**:S	His183:HE2	His183:NE2	85.40	3.19
4	Compd. **4**:S	Tyr306:HH	Tyr306:OH	100.00	2.95
5	Compd. **5**:S	Tyr308:HH	Tyr308:OH	100.00	2.91
6	Compd. **6**:S	Tyr308:HH	Tyr308:OH	100.00	2.90
7	Compd. **7**:S	Tyr308:HH	Tyr308:OH	100.00	2.98
8	Compd. **8**:S	Tyr308:HH	Tyr308:OH	100.00	2.88
	Compd. **8**:O_2	Phe210:H	Phe210:N	68.20	3.08
9	Compd. **9**:S	Tyr308:HH	Tyr308:OH	100.00	2.96
10	Compd. **10**:S	Tyr308:HH	Tyr308:OH	100.00	2.94
11	Compd. **11**:S	Tyr308:HH	Tyr308:OH	100.00	2.92
	Compd. **11**:O_2	Phe210:H	Phe210:N	15.60	3.20
12	Compd. **12**:S	Tyr308:HH	Tyr308:OH	100.00	2.89
13	Compd. **13**:S	Tyr308:HH	Tyr308:OH	100.00	2.94
	Compd. **13**:O_2	His183:HE2	His183:NE2	33.60	2.94

3. Conclusions

We successfully synthesized a series of HDACIs with differences in the surface recognition domains, and all compounds showed potent HDAC-inhibitory abilities and anti-proliferative activities against cancer cells. The introduction of 2-amino-4-phenylthiazole or 9-methyleneoxy-fluorenyl group at the surface recognition domain could largely increase their HDAC-inhibitory activity. Docking studies showed that changes in the structures of these compounds could affect the mode of their binding with HDACs. MD simulations revealed that zinc coordination, formation of hydrogen bond and the presence of hydrophobic effect contributed to the strong inhibitory activity of these compounds toward HDACs. Asp181, Asp269, Leu276 and Tyr308 of HDAC2 contributed favorably to the binding between enzyme and each of the compounds, so these amino acids should have an important effect on deacetylation ability of HDAC2. The results obtained from molecular modeling were in accordance with the HDAC-inhibitory activity profiles, so therefore could be considered as a reliable method available for the designing and screening of new HDACIs that have similar structures with this series compounds. The information obtained from this study would provide new insight into the mechanism of the interaction between inhibitors and HDACs, which could assist with the rational design of some novel and potent HDACIs for medical application.

Table 4
Binding free energies of all compounds to HDAC2 from MD simulations.

Compd.	ΔE_{int}^{ele}	ΔE_{int}^{vdw}	ΔE_{int}	ΔG_{sol}^{nonpol}	ΔG_{sol}^{ele}	ΔG_{sol}	ΔG_{ele}	ΔG_b
1	−68.80	−30.07	−98.87	−5.79	95.11	89.31	26.31	−9.55
2	−63.59	−30.03	−93.62	−5.07	88.8	83.73	25.21	−9.89
3	−69.62	−34.41	−104.03	−6.61	94.83	88.23	25.21	−15.80
4	−70.36	−30.28	−100.64	−6.75	98.98	92.24	28.62	−8.40
5	−68.87	−28.79	−97.66	−6.60	96.50	89.9	27.63	−7.76
6	−64.18	−28.25	−92.43	−5.66	90.12	84.47	25.94	−7.96
7	−69.86	−28.95	−98.81	−5.48	96.31	90.83	26.45	−7.98
8	−68.19	−34.9	−103.09	−5.45	92.42	86.97	24.23	−16.12
9	−77.63	−27.89	−105.52	−6.06	103.67	97.61	26.04	−7.91
10	−75.53	−26.02	−101.55	−5.81	98.06	92.25	22.53	−9.30
11	−64.03	−36.80	−100.83	−5.38	96.72	91.34	32.69	−9.49
12	−63.37	−34.66	−98.03	−5.23	93.7	88.47	30.33	−9.56
13	−68.97	−34.64	−103.61	−6.09	98.44	92.35	29.47	−11.26

4. Experiments and computational methodology

4.1. Synthesis

4.1.1. Instruments and materials

Thin layer chromatography (TLC) and/or high performance liquid chromatography (HPLC) were used to check all intermediate products and target compounds. TLC was performed on aluminum-backed silica gel plates (Merck DC-Alufolien Kieselgel 60 F254) and the spots were visualized by ultraviolet light or charring. Analytical HPLC was performed on Jasco PU-1586 using a Chromolith Performance RP-18e column (4.6 × 100 mm, Merck). The mobile phases used were A: H_2O with 10% CH_3CN and 0.1% trifluoroacetic acid (TFA); B: CH_3CN with 0.1% TFA. Elution of the desired compounds was carried out using a solvent gradient of A to B over 15 min at a flow rate of 2 mL/min. Eluent was detected at 220 nm. High-resolution mass spectrometry (HRMS) were measured on a UPLC/Q-Tof Mass Spectrometer instrument. Nuclear magnetic resonance (NMR) spectra were recorded on a Varian INOVA 400 MHz spectrometer.

4.1.2. Synthesis of L-Ab8

L-Ab8 was synthesized according to the procedure reported in ref. [21] using diethyl acetamidomalonate and 1, 6-dibromohexan as starting material.

4.1.3. Synthesis of compound *1*

To a solution of L-Ab8 (714 mg) in H_2O (3 mL), Na_2CO_3 (382 mg), acetone (3 mL) and N-(benzyloxycarbonyloxy) succinimide (Z-OSu) (897 mg) were added and stirred for 5 h. The progress of the reaction was monitored by TLC ($CHCl_3$:CH_3OH:CH_3COOH = 90:10:2) and HPLC. After the reaction had completed, the acetone was evaporated and the residue was washed with aether. Citric acid was added until the pH reached 3.0. The residue was then dissolved in ethyl acetate and then washed in sodium bicarbonate solution (4%) and brine, and dried over anhydrous $MgSO_4$. Z-L-Ab8 was obtained as oil after ethyl acetate was evaporated (1.04 g, 93.2%). To a solution of Z-L-Ab8 (1.04 g) in ^{t}Bu—OH (14 mL), Boc anhydride (1.22 g) and 4-dimethylamiopryidine (DMAP) (34 mg) were added. After the reaction had completed as monitored by TLC ($CHCl_3$:CH_3OH = 9:1) and HPLC, the ^{t}Bu—OH was evaporated and the residue was purified by silica gel chromatography using a mixture of hexane and ethyl acetate (8:1) to yield Z-L-Ab8-O^{t}Bu (1.08 g, 90.2%). The side chain of Z-L-Ab8-O^{t}Bu was changed from a bromo group to a thioacetyl group by treatment with potassium thioacetate (433 mg) in N,N-dimethylformamide (DMF) for 5 h. The thioester was extracted as before to yield Z-L-Am8(SAc)-O^{t}Bu (1.0 g, 93.3%). The compound was then dissolved in DMF, and 2, 2′-dipyridyldisulfide (624 mg) was added, followed by 40% solution of CH_3NH_2/CH_3OH (1.27 mL) under argon atmosphere and stirred for 6 h. After evaporation of DMF, the residue was extracted and purified by silica gel chromatography using mixture of dichloromethane (DCM) and methanol (149:1) to yield Z-L-Am8(S2Py)-O^{t}Bu as powder (743 mg, 64.2%). The compound was dissolved in TFA (1.5 mL) at 0 °C and kept for 2 h. TFA in the sample was evaporated and Z-Am8(S2Py)-OH was obtained as a yellow oil (661 mg, 100%). Z-Am8(S2Py)-OH (217 mg) was coupled with 1-naphthylamine (72 mg) in cooled DMF, and N-hydroxybenzotrizole (HOBt·H_2O) (92 mg), 2-(1H-benzotriazole-1-yl)-1,1,3,3-tetramethyluronium hexafluorophosphate (HBTU) (228 mg), and N,N-diisopropylethylamine (DIEA) (87 μL) were added and

Table 5
Contributions of the amino acid residues in the active site of HDAC2 to the binding free energy (kcal/mol).

Compd.	Amino acid residues								
	His145	His146	Gly154	Phe155	Asp181	His183	Asp269	Leu276	Tyr308
1	1.22	9.02	1.29	6.02	−69.01	0.45	−63.11	−20.29	−19.28
2	3.68	1.52	0.14	6.55	−64.20	3.16	−59.51	−22.08	−19.57
3	2.92	4.57	0.35	5.67	−64.45	7.33	−61.51	−21.70	−19.73
4	1.02	4.20	0.87	7.25	−67.72	2.16	−62.78	−20.96	−18.38
5	1.06	6.17	0.33	6.14	−63.65	4.13	−59.89	−21.70	−20.40
6	1.71	3.22	0.50	6.49	−64.26	3.27	−59.83	−21.12	−20.52
7	4.11	5.40	0.60	5.20	−67.81	2.59	−64.79	−20.27	−19.72
8	1.20	7.88	−0.88	6.37	−63.04	3.43	−59.69	−22.91	−19.92
9	2.22	6.10	−0.14	6.73	−66.23	4.02	−62.77	−20.00	−19.31
10	3.50	5.44	0.89	6.54	−66.11	3.32	−62.25	−20.27	−20.76
11	1.08	−0.07	0.13	6.79	−61.57	3.15	−55.91	−23.31	−19.71
12	1.33	−0.07	−0.10	6.43	−63.67	4.35	−59.25	−20.87	−19.74
13	0.63	8.35	1.04	5.86	−68.48	−0.53	−61.28	−22.29	−19.88

stirred overnight. After the reaction had completed as monitored by TLC ($CHCl_3$:CH_3OH = 9:1) and HPLC, the DMF was evaporated and the residue was dissolved in ethyl acetate and washed with citric acid solution (10%), followed by sodium bicarbonate solution (4%) and brine, and then dried over anhydrous $MgSO_4$. The remaining ethyl acetate was evaporated and the residue was purified by silica gel chromatography using a mixture of DCM and methanol (149:1) to yield compound **1** (256 mg, 91.5%; Overall yield: 46.1%) as a white solid. M.p. 111–113 °C. HPLC purity: 98.2%. HRMS: $[M + Na]^+$ 582.1866 for $C_{31}H_{33}N_3O_3S_2$ (calcd 582.1861); ^1H NMR ($CDCl_3$, 400 MHz, δ, ppm) 8.44 (1H, d, J = 4.1 Hz), 7.83 (3H, m), 7.69 (1H, d, J = 8.0 Hz), 7.64 (2H, m), 7.44 (2H, t, J = 4.6 Hz), 7.38 (1H, t, J = 7.8 Hz), 7.28 (5H, m), 7.04 (1H, t, J = 5.7 Hz), 5.68 (1H, d, J = 7.7 Hz), 5.10 (2H, t, J = 12.9 Hz), 4.49 (1H, s), 2.75 (2H, t, J = 7.1 Hz), 1.97 (1H, t, J = 6.7 Hz), 1.74 (1H, t, J = 7.7 Hz), 1.66 (2H, t, J = 6.8 Hz), 1.36 (7H, m); ^{13}C NMR ($CDCl_3$, 400 MHz, δ, ppm) 170.78, 160.59, 156.80, 153.33, 149.58, 137.05, 135.97, 134.07, 132.03, 128.63, 128.59, 128.30, 128.04, 127.20, 126.39, 126.02, 125.96, 125.61, 120.93, 120.90, 120.59, 119.67, 67.37, 55.75, 38.77, 32.13, 28.84, 28.73, 28.20, 25.54.

4.1.4. Synthesis of compound **2**

This compound was synthesized according to the procedure reported for compound **1** using cyclohexylamine instead of 1-naphthylamine. Compound **2** yield 41.1% as a white solid. M.p 78–80 °C. HPLC purity: 97.8%. HRMS: $[M + Na]^+$ 538.2165 for $C_{27}H_{37}N_3O_3S_2$ (calcd 538.2174); ^1H NMR ($CDCl_3$, 400 MHz, δ, ppm) 8.46 (1H, d, J = 4.5 Hz), 7.71 (1H, d, J = 8.0 Hz), 7.65 (1H, t, J = 7.1 Hz), 7.35 (4H, m), 7.26 (1H, s), 7.08 (1H, t, J = 5.8 Hz), 5.77 (1H, d, J = 8.6 Hz), 5.29 (1H, d, J = 6.8 Hz), 5.10 (1H, s), 4.03 (1H, d, J = 7.2 Hz), 3.74 (1H, s), 2.77 (1H, t, J = 7.2 Hz), 1.87 (1H, t, J = 7.9 Hz), 1.78 (1H, t, J = 7.5 Hz), 1.67 (3H, m), 1.61 (5H, m) 1.30 (9H, m), 1.13 (3H, m); ^{13}C NMR ($CDCl_3$, 400 MHz, δ, ppm) 170.47, 160.60, 156.13, 149.61, 137.01, 136.25, 128.58, 128.25, 128.11, 120.57, 119.64, 67.04, 55.09, 48.32, 38.76, 33.06, 32.93, 32.72, 29.74, 28.76, 28.70, 28.16, 25.47, 25.24, 24.77.

4.1.5. Synthesis of compound **3**

This compound was synthesized according to the procedure reported for compound **1** using 2-amino-4-phenylthiazole hydrobromide monohydrate instead of 1-naphthylamine. Compound **3** yield 44.0% as a light yellow solid. M.p 76–78 °C. HPLC purity: 98.5%. HRMS: $[M + Na]^+$ 615.1528 for $C_{30}H_{32}N_4O_3S_3$ (calcd 615.1534); ^1H NMR ($CDCl_3$, 400 MHz, δ, ppm) 8.46 (1H, d, J = 4.7 Hz), 7.79 (1H, d, J = 1.3 Hz), 7.76 (1H, s), 7.70 (1H, d, J = 8.2 Hz), 7.63 (1H, t, J = 7.9 Hz), 7.36 (7H, m), 7.26 (1H, s), 7.14 (1H, s), 7.07 (1H, t, J = 5.8 Hz), 5.47 (1H, d, J = 7.7 Hz), 5.16 (1H, q, J = 12.1 Hz), 4.52 (1H, d, J = 7.0 Hz), 2.75 (2H, t, J = 7.2 Hz), 1.92 (1H, s), 1.66 (3H, m), 1.34 (7H, m) 1.00 (1H, d, J = 6.7 Hz); ^{13}C NMR ($CDCl_3$, 400 MHz, δ, ppm) 170.28, 167.72, 160.59, 157.80, 156.49, 149.56, 137.07, 135.79, 133.57, 132.38, 130.95, 128.83, 128.62, 128.40, 128.30, 126.15, 120.61, 119.76, 107.96, 71.83, 67.72, 55.13, 38.69, 32.06, 29.74, 28.67, 28.06, 27.75, 25.27, 19.20.

4.1.6. Synthesis of compound **4**

This compound was synthesized according to the procedure reported for compound **1** using 2-aminobiphenyl instead of 1-naphthylamine. Compound **4** yield 47.2% as a white solid. M.p 112–114 °C. HPLC purity: 98.8%. HRMS: $[M + Na]^+$ 608.2026 for $C_{33}H_{35}N_3O_3S_2$ (calcd 608.2018); ^1H NMR ($CDCl_3$, 400 MHz, δ, ppm) 8.44 (1H, d, J = 3.1 Hz), 8.29 (1H, d, J = 7.9 Hz), 7.72 (2H, t, J = 7.6 Hz), 7.63 (1H, t, J = 7.0 Hz), 7.34 (9H, m), 7.26 (2H, d, J = 7.1 Hz), 7.21 (1H, d, J = 7.3 Hz), 7.06 (1H, t, J = 5.2 Hz), 5.15 (1H, s), 5.07 (1H, q, J = 11.7 Hz), 4.08 (1H, s), 2.75 (1H, t, J = 6.8 Hz), 1.61 (4H, m), 1.25 (9H, m); ^{13}C NMR ($CDCl_3$, 400 MHz, δ, ppm) 169.64, 160.57, 155.96, 149.61, 137.85, 136.99, 136.02, 134.18, 132.60, 130.09, 129.23, 129.12, 128.59, 128.48, 128.32, 128.12, 128.07, 124.67, 121.34, 120.56, 119.65, 67.20, 55.80, 38.77, 32.41, 29.73, 28.73, 28.70, 28.15, 25.16.

4.1.7. Synthesis of compound **5**

This compound was synthesized according to the procedure reported for compound **1** using 4-aminobiphenyl instead of 1-naphthylamine. Compound **5** yield 45.7% as a white solid. M.p 114–116 °C. HPLC purity: 98.1%. HRMS: $[M + Na]^+$ 608.2012 for $C_{33}H_{35}N_3O_3S_2$ (calcd 608.2018); ^1H NMR ($CDCl_3$, 400 MHz, δ, ppm) 8.45 (1H, d, J = 2.5 Hz), 8.30 (1H, s), 7.71 (1H, d, J = 7.7 Hz), 7.63 (1H, t, J = 7.7 Hz), 7.54 (5H, m), 7.42 (2H, t, J = 7.0 Hz), 7.35 (5H, m), 7.26 (1H, s), 7.07 (1H, t, J = 4.4 Hz), 5.41 (1H, d, J = 5.8 Hz), 5.14 (2H, t, J = 11.7 Hz), 4.28 (1H, s), 2.76 (2H, t, J = 6.4 Hz), 1.95 (1H, t, J = 7.6 Hz), 1.64 (4H, m), 1.38 (6H, m); ^{13}C NMR ($CDCl_3$, 400 MHz, δ, ppm) 170.00, 160.61, 156.66, 149.61, 140.46, 137.40, 137.05, 136.83, 135.97, 128.80, 128.64, 128.37, 128.14, 127.62, 127.17, 126.87, 120.61, 120.28, 119.73, 67.42, 55.79, 38.67, 31.99, 28.65, 28.07, 25.37.

4.1.8. Synthesis of compound **6**

Z-Am8(S2Py)-OH was obtained as described above. Z-Am8(S2Py)-OH (217 mg) was coupled with 4-biphenylmethanol (111 mg) in DMF by the aid of DMAP (6.1 mg) and dicyclohexylcarbodiimide (DCC) (124 mg) and stirred for 8 h. After the reaction had completed as monitored by TLC ($CHCl_3$:CH_3OH = 9:1) and HPLC, the DMF was evaporated and the residue was dissolved in ethyl acetate and washed with citric acid solution (10%), followed by sodium bicarbonate solution (4%) and brine, and then dried over anhydrous $MgSO_4$. The remaining ethyl acetate was evaporated and the residue was purified by silica gel chromatography using a mixture of DCM and methanol (149:1) to yield compound **6** (272 mg, 90.7%; Overall yield: 46.0) as a colorless oil. HPLC purity: 97.9%. HRMS: $[M + Na]^+$ 623.2001 for $C_{34}H_{36}N_2O_4S_2$ (calcd 623.2014); ^1H NMR ($CDCl_3$, 400 MHz, δ, ppm) 8.45 (1H, d, J = 4.4 Hz), 7.68 (1H, d, J = 8.1 Hz), 7.58 (5H, m), 7.42 (4H, q, J = 7.8 Hz), 7.35 (6H, m), 7.06 (1H, t, J = 6.5 Hz), 5.11 (1H, s), 2.71 (1H, t, J = 7.2 Hz), 1.61 (5H, m), 1.26 (9H, m), 0.98 (2H, d, J = 6.7 Hz); ^1H NMR ($CDCl_3$, 400 MHz, δ, ppm); ^{13}C NMR ($CDCl_3$, 400 MHz, δ, ppm) 172.43, 167.71, 160.60, 155.87, 149.61, 141.48, 140.51, 136.97, 136.24, 134.28, 132.39, 130.95, 128.87, 128.57, 128.24, 128.16, 127.56, 127.38, 127.13, 120.53, 119.59, 71.83, 67.04, 66.91, 53.90, 38.82, 32.62, 29.74, 28.71, 28.18, 27.75, 24.93, 19.20.

4.1.9. Synthesis of compound **7**

This compound was synthesized according to the procedure reported for compound **1** using 9-aminofluorene hydrochloride instead of 1-naphthylamine. Compound **7** yield 40.8% as a light yellow solid. M.p 130–132 °C. HPLC purity: 98.6%. HRMS: $[M + Na]^+$ 620.2023 for $C_{34}H_{35}N_3O_3S_2$ (calcd 620.2018); ^1H NMR ($CDCl_3$, 400 MHz, δ, ppm) 8.42 (1H, s), 7.64 (4H, m), 7.48 (2H, s), 7.37 (3H, t, J = 7.3 Hz), 7.30 (6H, m), 7.05 (1H, s), 6.51 (1H, s), 6.17 (1H, d, J = 8.0 Hz), 5.43 (1H, s), 4.92 (1H, s), 4.23 (1H, s), 2.77 (1H, t, J = 6.3 Hz), 1.87 (1H, t, J = 5.0 Hz), 1.66 (3H, s), 1.35 (8H, m); ^{13}C NMR ($CDCl_3$, 400 MHz, δ, ppm) 172.55, 160.57, 156.05, 149.59, 144.06, 143.86, 140.61, 136.98, 136.07, 128.79, 128.54, 128.24, 128.08, 127.85, 125.07, 125.00, 120.55, 120.05, 119.65, 67.03, 55.14, 54.70, 38.76, 32.91, 29.73, 28.77, 28.70, 28.19, 25.27.

4.1.10. Synthesis of compound **8**

This compound was synthesized according to the procedure reported for compound **6** using 9-fluorenemethanol instead of 4-biphenylmethanol. Compound **8** yield 44.5% as a light yellow oil. HPLC purity: 98.3%. HRMS: $[M + Na]^+$ 635.2026 for $C_{35}H_{36}N_2O_4S_2$ (calcd 635.2014); ^1H NMR ($CDCl_3$, 400 MHz, δ, ppm) 8.47 (1H, d, J = 4.6 Hz), 7.75 (2H, m), 7.58 (2H, m), 7.41 (1H, m), 7.35 (2H, t, J = 8.8 Hz), 7.26 (8H, m), 7.07 (1H, t, J = 6.9 Hz), 5.12 (1H, s), 4.51 (1H,

d, $J = 6.8$ Hz), 4.20 (1H, t, $J = 5.1$ Hz), 2.78 (1H, t, $J = 6.9$ Hz), 1.67 (2H, t, $J = 8.2$ Hz), 1.55 (10H, m), 1.26 (3H, s); ^{13}C NMR ($CDCl_3$, 400 MHz, δ, ppm) 172.28, 160.48, 155.96, 150.25, 149.59, 147.80, 142.55, 138.53, 137.05, 136.15, 128.58, 128.47, 128.29, 128.13, 127.58, 123.88, 120.98, 120.60, 119.64, 67.12, 65.50, 53.91, 38.72, 36.62, 32.34, 29.72, 28.92, 28.66, 28.61, 28.35, 28.11, 25.11, 25.00.

4.1.11. Synthesis of compound **9**

Z-Am8(S2Py)-OH was obtained as described above. Z-Am8(S2Py)-OH (217 mg) was coupled with 4-nitrobenzyl bromide (130 mg) in cooled DMF, triethylamine (84 μL) was added and the solution was stirred overnight. After the reaction had completed as monitored by TLC ($CHCl_3$:CH_3OH = 9:1) and HPLC, the DMF was evaporated and the residue was dissolved in ethyl acetate and washed with citric acid solution (10%), followed by sodium bicarbonate solution (4%) and brine, and then dried over anhydrous $MgSO_4$. The remaining ethyl acetate was evaporated and the residue was purified by silica gel chromatography using a mixture of DCM and methanol (149:1) to yield compound **9** (273 mg, 95.8%; Overall yield: 48.3%) as a light yellow oil. HPLC purity: 97.7%. HRMS: $[M + Na]^+$ 592.1560 for $C_{28}H_{31}N_3O_6S_2$ (calcd 592.1552); ^{1}H NMR ($CDCl_3$, 400 MHz, δ, ppm) 8.46 (1H, d, $J = 4.7$ Hz), 8.19 (2H, d, $J = 8.3$ Hz), 7.70 (1H, d, $J = 8.0$ Hz), 7.64 (1H, t, $J = 6.6$ Hz), 7.50 (2H, d, $J = 8.3$ Hz), 7.34 (5H, m), 7.07 (1H, t, $J = 5.1$ Hz), 5.26 (2H, s), 5.11 (2H, s), 4.42 (1H, d, $J = 5.2$ Hz), 2.76 (1H, t, $J = 7.2$ Hz), 1.83 (1H, t, $J = 7.3$ Hz), 1.66 (3H, m), 1.32 (8H, m); ^{13}C NMR ($CDCl_3$, 400 MHz, δ, ppm) 172.28, 160.48, 155.96, 149.59, 147.80, 142.55, 137.05, 136.15, 128.58, 128.47, 128.29, 128.13, 123.88, 120.60, 119.64, 67.12, 65.50, 53.91, 38.72, 36.62, 32.34, 28.92, 28.66, 28.61, 28.35, 28.11, 25.11, 25.00.

4.1.12. Synthesis of compound **10**

This compound was synthesized according to the procedure reported for compound **9** using 3-nitrobenzyl bromide instead of 4-nitrobenzyl bromide. Compound **10** yield 47.0% as a light yellow oil. HPLC purity: 98.5%. HRMS: $[M + Na]^+$ 592.1564 for $C_{28}H_{31}N_3O_6S_2$ (calcd 592.1552); ^{1}H NMR ($CDCl_3$, 400 MHz, δ, ppm) 8.46 (1H, d, $J = 4.5$ Hz), 8.21 (2H, d, $J = 10.2$ Hz), 7.70 (3H, m), 7.55 (1H, t, $J = 7.7$ Hz), 7.35 (5H, m), 7.07 (1H, t, $J = 6.6$ Hz), 5.26 (2H, d, $J = 3.7$ Hz), 5.11 (2H, s), 4.43 (1H, d, $J = 5.4$ Hz), 2.75 (1H, t, $J = 7.2$ Hz), 1.84 (1H, t, $J = 7.9$ Hz), 1.67 (4H, m), 1.29 (7H, m); ^{13}C NMR ($CDCl_3$, 400 MHz, δ, ppm) 172.28, 160.54, 155.92, 149.61, 148.38, 137.44, 137.01, 136.15, 134.00, 129.77, 128.57, 128.27, 128.16, 123.42, 122.93, 120.56, 119.62, 67.13, 65.57, 53.88, 38.74, 32.41, 28.67, 28.62, 28.12, 25.06.

4.1.13. Synthesis of compound **11**

This compound was synthesized according to the procedure reported for compound **9** using 2-(bromomethyl)naphthalene instead of 4-nitrobenzyl bromide. Compound **11** yield 48.1% as a light yellow oil. HPLC purity: 98.0%. HRMS: $[M + Na]^+$ 597.1853 for $C_{32}H_{34}N_2O_4S_2$ (calcd 597.1858); ^{1}H NMR ($CDCl_3$, 400 MHz, δ, ppm) 8.45 (1H, d, $J = 4.5$ Hz), 8.01 (1H, s), 7.70 (3H, t, 3.9 Hz), 7.68 (1H, d, $J = 8.0$ Hz), 7.62 (1H, t, $J = 6.7$ Hz), 7.50 (2H, m), 7.44 (1H, d, $J = 8.3$ Hz), 7.34 (4H, m), 7.12 (1H, t, $J = 5.8$ Hz), 7.06 (1H, t, $J = 6.4$ Hz), 5.36 (1H, d, $J = 12.2$ Hz), 5.30 (1H, t, $J = 9.8$), 5.11 (1H, s), 4.44 (1H, d, $J = 5.7$ Hz), 2.95 (1H, s), 2.88 (1H, s), 2.69 (1H, t, $J = 7.3$ Hz), 1.81 (1H, d, $J = 7.8$), 1.58 (3H, m), 1.26 (7H, m); ^{13}C NMR ($CDCl_3$, 400 MHz, δ, ppm) 172.42, 162.56, 160.62, 158.98, 155.88, 149.60, 137.43, 136.97, 136.24, 133.20, 133.13, 132.73, 128.56, 128.22, 128.14, 128.03, 127.75, 126.44, 125.89, 121.13, 120.53, 119.59, 67.29, 67.03, 53.91, 38.81, 36.52, 32.59, 29.74, 28.66, 28.13, 24.89.

4.1.14. Synthesis of compound **12**

This compound was synthesized according to the procedure reported for compound **6** using 1-naphthalenemethanol instead of 4-biphenylmethanol. Compound **12** yield 41.9% as a light yellow oil. HPLC purity: 98.7%. HRMS: $[M + Na]^+$ 597.1863 for $C_{32}H_{34}N_2O_4S_2$ (calcd 597.1858); ^{1}H NMR ($CDCl_3$, 400 MHz, δ, ppm) 8.46 (1H, d, $J = 4.3$ Hz), 8.00 (1H, d, $J = 8.0$ Hz), 7.87 (2H, t, 7.4 Hz), 7.69 (1H, d, $J = 8.1$ Hz), 7.62 (1H, t, $J = 7.2$ Hz), 7.52 (2H, m), 7.44 (1H, t, $J = 7.3$ Hz), 7.34 (4H, m), 7.26 (1H, s), 7.11 (1H, t, $J = 4.8$ Hz), 7.06 (1H, t, $J = 6.5$ Hz), 5.68 (1H, s), 5.58 (1H, s), 5.28 (1H, d, $J = 8.2$ Hz), 5.01 (1H, s), 4.41 (1H, d, $J = 6.1$ Hz), 2.70 (1H, t, $J = 7.4$ Hz), 1.64 (6H, m), 1.26 (2H, s), 1.15 (3H, m), 1.06 (1H, m); ^{13}C NMR ($CDCl_3$, 400 MHz, δ, ppm) 172.41, 160.63, 155.82, 149.60, 137.43, 136.97, 136.23, 133.75, 131.61, 130.80, 129.66, 128.80, 128.55, 128.21, 128.13, 128.02, 126.70, 126.07, 125.26, 123.48, 120.53, 119.60, 67.01, 65.56, 53.91, 38.83, 32.53, 30.95, 28.64, 28.58, 28.08, 24.77.

4.1.15. Synthesis of compound **13**

This compound was synthesized according to the procedure reported for compound **6** using 9-anthracenemethanol instead of 4-biphenylmethanol. Compound **13** yield 43.8% as a light yellow oil. HPLC purity: 98.1%. HRMS: $[M + Na]^+$ 647.2030 for $C_{36}H_{36}N_2O_4S_2$ (calcd 647.2014); ^{1}H NMR ($CDCl_3$, 400 MHz, δ, ppm) 8.51 (1H, s), 8.45 (1H, d, $J = 4.5$ Hz), 8.31 (1H, d, $J = 8.8$ Hz), 8.02 (1H, d, $J = 8.4$ Hz), 7.66 (1H, d, $J = 8.1$ Hz), 7.58 (2H, m), 7.49 (2H, t, $J = 7.8$ Hz), 7.32 (5H, m), 7.26 (1H, s), 7.05 (1H, t, $J = 5.4$ Hz), 6.33 (1H, d, $J = 12.6$ Hz), 6.11 (1H, d, $J = 12.5$ Hz), 5.25 (1H, d, $J = 7.8$ Hz), 5.07 (2H, t, $J = 12.1$ Hz), 4.39 (1H, d, $J = 6.1$ Hz), 2.63 (1H, t, $J = 7.2$ Hz), 1.63 (4H, m), 1.45 (1H, m), 1.26 (2H, s), 1.04 (6H, m); ^{13}C NMR ($CDCl_3$, 400 MHz, δ, ppm) 172.70, 160.65, 155.80, 149.59, 136.96, 136.23, 131.35, 131.03, 129.52, 129.19, 128.54, 128.19, 128.12, 126.82, 125.58, 125.20, 123.81, 120.51, 119.57, 66.98, 59.86, 53.91, 38.81, 32.51, 29.73, 28.55, 28.49, 28.01, 24.72, 19.19.

4.2. HDAC-inhibitory assay

HDAC-inhibitory activities of all compounds were assayed with the Biomol AK511 (containing human HDAC1) and AK500 (containing HeLa nuclear extract, rich in HDAC1 and HDAC2) kits to determine IC_{50} values against HDAC1 and HDAC2, and the assay was performed according to the manufacturer's instructions in triplicate and repeated three times. The disulfide bond of each compound was reduced by dithiothreitol (DTT) to give a thiol group that acts as metal binding domain before the assay.

4.3. Cell growth inhibitory assay

Growth inhibition was determined using a standard MTT assay. MCF-7 was cultured in DMEM medium supplemented with 10% fatal bovine serum. Cell cultures were incubated at 37 °C with 5% CO_2 in air. Cells were diluted to 5–9 × 10^4 cells/mL with medium and plated in a 96-well plate. After overnight incubation, aliquot of 10-time serial dilution of each compound to be evaluated was added, and the plate was incubated for 48 h. Then 200 μL MTT solution diluted in serum free medium (0.5 mg/mL) was added to each well and the cells were incubated for an additional 4 h followed by addition of 200 μL DMSO to dissolve the dark blue crystal (formazan). The plate was then read at 570 nm using a spectrophotometer. The IC_{50} values were determined in triplicate and the experiment was repeated at least three times.

4.4. Docking studies

AutoDock4.0 program [22,23] was used in the docking studies. Initial X-ray structure of HDAC2 was obtained from the Protein Data Bank (PDB) (PDB ID: 3MAX). The disulfide bonds in the metal biding domains of inhibitors were changed to thiol groups in docking, because the thiol group was the active group that interacted with

enzymes. The inhibitors were put into the active pocket of HDAC2, and the grid maps were centered on the inhibitors and comprised $70 \times 70 \times 70$ points with 0.375 Å spacing. For all inhibitors, all the single bonds except the amide bonds were treated as active torsional bonds. Lamarckian genetic algorithm was used with a maximum number of 25,000,000 energy evaluations and a maximum number of 5000 generations for each run. The other parameters were all set as default in AutoDock4.0. For all calculations, 150 docking runs were performed. Results differed by less than 2.0 Å in positional root-mean-square deviation (RMSD) were clustered together. The best docking results were chosen for MD simulations. The LigPlot program [24] was employed to analyze the docking results that focused on hydrogen bonding and hydrophobic interactions.

4.5. MD simulations

HDAC2-compound complexes were used for further MD simulations to understand how the compounds bind to HDAC2 in explicit aqueous solution. The initial structures for the simulations were obtained from docked conformations. The AMBER9 [25] package was used for all molecular mechanics and dynamics calculations. The standard AMBER ff99 force field [26] parameters were assigned to enzyme and water atoms, and the general AMBER force field (GAFF) [27] were used for the inhibitors. Zinc ion was modeled using the Stote non-bonded model ($q = +2e^{-}$, $r = 1.7$ Å, $\varepsilon = 0.67$ kcal/mol) [28]. The local hydrogen bonding network around the histidine residues was checked. His183 of HDAC2 was assigned as HIE (histidine with hydrogen on its epsivlon nitrogen), and other histidine residues as HID (histidine with hydrogen on its delta nitrogen). The force field parameters of all inhibitors were prepared with the Antechamber module [29] of AMBER9 package. Atomic charges of the inhibitors were derived with the AM1-BCC charge method [30]. Hydrogen atoms were added to the crystallographic HDAC2 with the AMBER Leap module. Sodium counterions were added to neutralize the system. The complex was then soaked in a truncated octahedron box of TIP3P [31] water molecules with a margin of 10 Å along each dimension. The particle mesh Ewald (PME) method [32] was applied to treat long-range electrostatic interactions. The cutoff distance for the long-range electrostatic and the van der Waals energy terms were set at 12.0 Å. All covalent bonds to hydrogen atoms were constrained using the SHAKE algorithm [33].

Energy minimization was achieved in three steps. In the first step, movement was allowed only for water molecules and counterions. In the second step, the inhibitor and the amino acid residues of HDAC2 were all allowed to move, while water molecules, together with counterions were constrained. In the final step, all atoms were permitted to move freely. In each step, energy minimization was executed by the steepest descent method for the first 5000 steps and by the conjugated gradient method for the subsequent 2500 steps. Periodic boundary conditions were used. The time steps were 2 fs during the production dynamics. The temperature was maintained by rescaling the velocities using the Berendsen weak-coupling algorithm [34], with a time constant of 2 ps for the heat bath. After the system was stepwise warmed-up from the initial 0 K–300 K using the NVT ensemble in 120 ps, molecular dynamics were performed at a constant temperature of 300 K. Each simulation was performed for 2 ns under periodic boundary conditions with NPT ensemble at a constant pressure of 1 atm.

The convergence of energies, temperatures, and pressures of the systems, and the atomic RMSD of HDAC2 and the inhibitor were used to verify the stability of the systems. Trajectories were analyzed using the PTRAJ modules [35]. In the present MD simulations, the overall structure of all complexes appeared to be equilibrated after 1.5 ns. Hence, atom coordinates for the last 500 ps were used to analyze the structure in detail.

4.6. Binding free energy calculations

For MM-PBSA methodology, snapshots were taken at 5 ps intervals from the corresponding 500 ps MD trajectories. Explicit water molecules were removed from the snapshots. The energy components were calculated using very large cutoff (999 Å). The binding free energy, ΔG_{bind}, was estimated as follows: $\Delta G_b = \Delta E_{\text{mm}} + \Delta G_{\text{sol}} - T\Delta S$ (1) where ΔE_{mm} is the molecular mechanics energy given by $\Delta E_{\text{mm}} = \Delta E_{\text{int}}^{\text{ele}} + \Delta E_{\text{int}}^{\text{vdw}}$ (2) where $\Delta E_{\text{int}}^{\text{ele}}$ and $\Delta E_{\text{int}}^{\text{vdw}}$ represent the HDAC2-inhibitor electrostatic and van der Waals interactions, respectively. The solvation free energy (ΔG_{sol}) was estimated as the sum of electrostatic solvation free energy ($\Delta E_{\text{sol}}^{\text{ele}}$) and non-polar solvation free energy ($\Delta G_{\text{sol}}^{\text{nonpol}}$): $\Delta G_{\text{sol}} = \Delta G_{\text{sol}}^{\text{ele}} + \Delta G_{\text{sol}}^{\text{nonpol}}$ (3) where $\Delta G_{\text{sol}}^{\text{ele}}$ was calculated using the Poisson–Boltzmann (PB) model and $\Delta G_{\text{sol}}^{\text{nonpol}}$ was determined with as a function of the solvent-accessible surface area [36]: $\Delta G_{\text{sol}}^{\text{nonpol}} = \gamma A + b$ where A is the solvent-accessible surface area estimated with the LCPO method [37] and the parameters $\gamma = 0.0072$ kcal/(mol Å^2) and $b = 0.0$ kcal/mol. The change in solute entropy upon complexation, $T\Delta S_{\text{conf}}$, was not estimated in this work. It seemed that entropy did not contribute much to the relative binding free energies of the ligands with similar to the same protein, and in some studies there have been good agreements between the experimental and calculated relative binding energies [38].

4.7. Binding free energy decomposition

MM-GBSA method was used for the binding energy calculation. This decomposition was used for molecular mechanics and solvation energies but not for entropies. Snapshots were taken at 5 ps time intervals from the last 500 ps MD trajectories. Explicit water molecules were removed from the snapshots. Energy decomposition was performed for gasphase energies (E_{gas}) and desolvation free energies (E_{sol}). The gasphase energies include internal energy (E_{int}), van der Waals energy (E_{vdw}) and electrostatic energy (E_{ele}). The polar contribution (ΔG_{gb}) of desolvation was computed using a modified GB model developed by Onufriev et al. [39] The LCPO method [37] was used to calculate the solvent-accessible surface area (SASA) for the estimation of the non-polar solvation free energy (ΔG_{np}) [36]. The total relative binding free energy of a given residue can be obtained by summing the contribution of each atom of this residue. The separate contribution of backbones and side-chains can be organized from the relevant atoms.

Acknowledgments

This work was supported by The National High Technology Research and Development Program of China (863 program), 2007AA021604. We thank Dr. Alan K Chang for his help with the revision of the manuscript.

References

[1] M. Grunstein, Histone acetylation in chromatin structure and transcription, Nature 389 (1997) 349–352.
[2] C. Hildmann, D. Riester, A. Schwienhorst, Histone deacetylases–an important class of cellular regulators with a variety of functions, Applied Microbiology and Biotechnology 75 (2007) 487–497.
[3] D.C. Drummond, C.O. Noble, D.B. Kirpotin, Z. Guo, G.K. Scott, C.C. Benz, Clinical development of histone deacetylase inhibitors as anticancer agents, Annual Review of Pharmacology and Toxicology 45 (2005) 495–528.

[4] A.J.M. De Ruijter, A.H. Van Gennip, H.N. Caron, S. Kemp, A.B.P. Van Kuilenburg, Histone deacetylases (HDACs): characterization of the classical HDAC family, Biochemical Journal 370 (2003) 737–749.
[5] M.S. Finnin, J.R. Donigian, A. Cohen, V.M. Richon, R.A. Rifkind, P.A. Marks, R. Breslow, N.P. Pavletich, Structures of a histone deacetylase homologue bound to the TSA and SAHA inhibitors, Nature 401 (1999) 188–193.
[6] J.R. Somoza, R.J. Skene, B.A. Katz, C. Mol, J.D. Ho, A.J. Jennings, C. Luong, A. Arvai, J.J. Buggy, E. Chi, J. Tang, B.C. Sang, E. Verner, R. Wynands, E.M. Leahy, D.R. Dougan, G. Snell, M. Navre, M.W. Knuth, R.V. Swanson, D.E. McRee, L.W. Tari, Structural snapshots of human HDAC8 provide insights into the class I histone deacetylases, Structure 12 (2004) 1325–1334.
[7] A.R. Gangloff, J.C. Bressi, A.J. Jennings, R. Skene, Y.Q. Wu, R. Melkus, R. De Jong, S. O'Connell, C.E. Grimshaw, M. Navre, Exploration of the HDAC2 foot pocket: synthesis and SAR of substituted *N*-(2-aminophenyl)benzamides, Bioorganic & Medicinal Chemistry Letters 20 (2010) 3142–3145.
[8] T. Jenuwein, C.D. Allis, Translating the histone code, Science 293 (2001) 1074–1080.
[9] P.A. Marks, R.A. Rifkind, V.M. Richon, R. Breslow, T. Miller, W.K. Kelly, Histone deacetylases and cancer: causes and therapies, Nature Reviews Cancer 1 (2001) 194–202.
[10] S. Minucci, P.G. Pelicci, Histone deacetylase inhibitors and the promise of epigenetic (and more) treatments for cancer, Nature Reviews Cancer 6 (2006) 38–51.
[11] H.E. Carraway, S.D. Gore, Addition of histone deacetylase inhibitors in combination therapy, Journal of Clinical Oncology 25 (2007) 1955–1956.
[12] V.M. Richon, S. Emiliani, E. Verdin, Y. Webb, R. Breslow, R.A. Rifkind, P.A. Marks, A class of hybrid polar inducers of transformed cell differentiation inhibits histone deacetylases, Proceedings of the National Academy of Sciences of the United States of America 95 (1998) 3003–3007.
[13] H. Ueda, T. Manda, S. Matsumoto, S. Mukumoto, F. Nishigaki, I. Kawamura, K. Shimomura, Fr901228, a Novel Antitumor Bicyclic Depsivpeptide Produced by Chromobacterium-Violaceum No-968 .3. Antitumor Activities on Experimental-Tumors in Mice, Journal of Antibiotics, 47 (1994) 315–323.
[14] A. Kuendgen, S. Knipp, F. Fox, C. Strupp, B. Hildebrandt, C. Steidl, U. Germing, R. Haas, N. Gattermann, Results of a phase 2 study of valproic acid alone or in combination with all-trans retinoic acid in 75 patients with myelodysplastic syndrome and relapsed or refractory acute myeloid leukemia, Annals of Hematology 84 (Suppl. 1) (2005) 61–66.
[15] T. Suzuki, T. Ando, K. Tsuchiya, N. Fukazawa, A. Saito, Y. Mariko, T. Yamashita, O. Nakanishi, Synthesis and histone deacetylase inhibitory activity of new benzamide derivatives, Journal of Medicinal Chemistry 42 (1999) 3001–3003.
[16] A. Saito, T. Yamashita, Y. Mariko, Y. Nosaka, K. Tsuchiya, T. Ando, T. Suzuki, T. Tsuruo, O. Nakanishi, A synthetic inhibitor of histone deacetylase, MS-27-275, with marked in vivo antitumor activity against human tumors, Proceedings of the National Academy of Sciences of the United States of America 96 (1999) 4592–4597.
[17] T.A. Miller, D.J. Witter, S. Belvedere, Histone deacetylase inhibitors, Journal of Medicinal Chemistry 46 (2003) 5097–5116.
[18] M. Yoshida, M. Kijima, M. Akita, T. Beppu, Potent and specific-inhibition of mammalian histone deacetylase both invivo and invitro by trichostatin-A, Journal of Biological Chemistry 265 (1990) 17174–17179.
[19] T. Suzuki, Y. Nagano, A. Kouketsu, A. Matsuura, S. Maruyama, M. Kurotaki, H. Nakagawa, N. Miyata, Novel inhibitors of human histone deacetylases: design, synthesis, enzyme inhibition, and cancer cell growth inhibition of SAHA-based non-hydroxamates, Journal of Medicinal Chemistry 48 (2005) 1019–1032.
[20] K.T. Hirashima Y, Nishino N, Maeda S, Nishino TG, Yoshida M., In Proceedings of 29th European Peptide Symposium (Peptides), (2006) 2.
[21] L.A. Watanabe, B. Jose, T. Kato, N. Nishino, M. Yoshida, Synthesis of L-alpha-amino-omega-bromoalkanoic acid for side chain modification, Tetrahedron Letters 45 (2004) 491–494.
[22] D.S. Goodsell, R. Huey, G.M. Morris, A.J. Olson, A semiempirical free energy force field with charge-based desolvation, Journal of Computational Chemistry 28 (2007) 1145–1152.
[23] G.M. Morris, D.S. Goodsell, R.S. Halliday, R. Huey, W.E. Hart, R.K. Belew, A.J. Olson, Automated docking using a Lamarckian genetic algorithm and an empirical binding free energy function, Journal of Computational Chemistry 19 (1998) 1639–1662.
[24] A.C. Wallace, R.A. Laskowski, J.M. Thornton, Ligplot - a program to generate schematic diagrams of protein ligand interactions, Protein Engineering 8 (1995) 127–134.
[25] D.A. Case, T.A. Darden, T.E. Cheatham, C.L. Simmerling, J. Wang, R.E. Duke, R. Luo, K.M. Merz, D.A. Pearlman, M. Crowley, R.C. Walker, W. Zhang, B. Wang, S. Hayik, A. Roitberg, G. Seabra, K.F. Wong, F. Paesani, X. Wu, S. Brozell, V. Tsui, H. Gohlke, L. Yang, C. Tan, J. Mongan, V. Hornak, G. Cui, P. Beroza, D.H. Mathews, C. Schafmeister, W.S. Ross, P.A. Kollman, AMBER Version 9, University of California, San Francisco, CA, 2006.
[26] J.M. Wang, P. Cieplak, P.A. Kollman, The ability of the AMBER ff99, Journal of Computational Chemistry 21 (2000) 1049–1074.
[27] J.M. Wang, R.M. Wolf, J.W. Caldwell, P.A. Kollman, D.A. Case, Development and testing of a general amber force field, Journal of Computational Chemistry 25 (2004) 1157–1174.
[28] R.H. Stote, M. Karplus, Zinc-binding in proteins and solution - a simple but accurate nonbonded representation, Proteins-Structure Function and Genetics 23 (1995) 12–31.
[29] J.M. Wang, W. Wang, P.A. Kollman, Antechamber: an accessory software package for molecular mechanical calculations, Abstracts of Papers of the American Chemical Society 222 (2001) U403.
[30] A. Jakalian, B.L. Bush, D.B. Jack, C.I. Bayly, Fast, efficient generation of high-quality atomic charges. AM1-BCC model: I. Method, Journal of Computational Chemistry 21 (2000) 132–146.
[31] W.L. Jorgensen, J. Chandrasekhar, J.D. Madura, R.W. Impey, M.L. Klein, Comparison of simple potential functions for simulating liquid water, Journal of Chemical Physics 79 (1983) 926–935.
[32] T. Darden, D. York, L. Pedersen, Particle mesh Ewald – an *N*Log(*N*) method for Ewald sums in large systems, Journal of Chemical Physics 98 (1993) 10089–10092.
[33] J.P. Ryckaert, G. Ciccotti, H.J.C. Berendsen, Numerical-integration of Cartesian equations of motion of a system with constraints – molecular-dynamics of *N*-alkanes, Journal of Computational Physics 23 (1977) 327–341.
[34] H.J.C. Berendsen, J.P.M. Postma, W.F. Vangunsteren, A. Dinola, J.R. Haak, Molecular-Dynamics with coupling to an external bath, Journal of Chemical Physics 81 (1984) 3684–3690.
[35] B. Honig, A. Nicholls, Classical electrostatics in biology and chemistry, Science 268 (1995) 1144–1149.
[36] D. Sitkoff, K.A. Sharp, B. Honig, Accurate calculation of hydration free-energies using macroscopic solvent models, Journal of Physical Chemistry 98 (1994) 1978–1988.
[37] J. Weiser, P.S. Shenkin, W.C. Still, Optimization of Gaussian surface calculations and extension to solvent-accessible surface areas, Journal of Computational Chemistry 20 (1999) 688–703.
[38] Z.G. Zhou, M. Madrid, J.D. Evanseck, J.D. Madura, Effect of a bound non-nucleoside RT inhibitor on the dynamics of wild-type and mutant HIV-1 reverse transcriptase, Journal of the American Chemical Society 127 (2005) 17253–17260.
[39] A. Onufriev, D. Bashford, D.A. Case, Modification of the generalized Born model suitable for macromolecules, Journal of Physical Chemistry B 104 (2000) 3712–3720.